



Recent Seismic Sequences and Activation of Normal Fault Systems in the Mugello Basin and Surrounding Areas (Northern Apennines, Italy)

Gilberto Saccorotti^{1*}, Rebecca Bruni^{1,2}, Marco Bonini³, Giacomo Corti³, Derek Keir^{4,5} and Federico Sani⁵

¹Istituto Nazionale di Geofisica e Vulcanologia, Sezione di Pisa, Pisa, Italy, ²Dipartimento di Scienze della Terra, Università di Pisa, Pisa, Italy, ³Consiglio Nazionale delle Ricerche, Istituto di Geoscienze e Georisorse, Sede Secondaria di Firenze, Firenze, Italy, ⁴School of Ocean and Earth Science, University of Southampton, Southampton, United Kingdom, ⁵Dipartimento di Scienze della Terra, Università degli Studi di Firenze, Firenze, Italy

OPEN ACCESS

Edited by:

Guillermo Booth-Rea,
University of Granada, Spain

Reviewed by:

Mikhail Rodkin,
Institute of Earthquake Prediction
Theory and Mathematical Geophysics
(RAS), Russia
Simone Cesca,
GFZ German Research Centre for
Geosciences, Germany

*Correspondence:

Gilberto Saccorotti
gilberto.saccorotti@ingv.it

Specialty section:

This article was submitted to
Solid Earth Geophysics,
a section of the journal
Frontiers in Earth Science

Received: 18 February 2022

Accepted: 04 April 2022

Published: 09 May 2022

Citation:

Saccorotti G, Bruni R, Bonini M,
Corti G, Keir D and Sani F (2022)
Recent Seismic Sequences and
Activation of Normal Fault Systems in
the Mugello Basin and Surrounding
Areas (Northern Apennines, Italy).
Front. Earth Sci. 10:879160.
doi: 10.3389/feart.2022.879160

The Mugello Basin (North-Eastern Tuscany) is an intermontane basin of the Northern Apennines (Italy) with a well-documented record of seismicity; the two major historical earthquakes occurred in 1542 (Mw = 6.0) and in 1919 (Mw = 6.4). In this study, we integrate different seismic catalogs spanning the 2005–2019 time interval, and complement these data with phase arrival times from a temporary network that specifically operated in the area throughout the 2019–2021 time interval. The subsequent relocation of this data set with a double-difference algorithm allows for accurate analyses of the most relevant seismic sequences which affected the study area in 2008, 2009, 2015–2017, and 2019. These sequences are associated with the activation of adjacent segments of larger NW-striking fault systems, one of which bounds the NE margin of the Mugello Basin (Ronta Fault System). For each seismic sequence, best-fit fault surfaces are derived from orthonormal regression of relocated hypocenters, yielding consistent results with that derived from fault plane solutions. The four sequences mark a significant increase in the seismicity rate with respect to what was recorded in the previous decades. This suggests that, following the 2008 renewal of seismicity, static or dynamic stress changes, or both depending on the case, played a role in advancing the time of failure of the fault segments activated subsequently.

Keywords: seismic sequence, fault segmentation, northern apennines, stress transfer, earthquake triggering

INTRODUCTION

Fault systems in geodynamically-active regions may extend over distances of hundreds or even thousands of kilometers, but only limited portions (segments) of those long fault zones rupture during strong earthquakes. The physical subdivision of a fault into segments is thought to be associated with specific geologic features that form barriers capable of slowing or even stopping the propagation of the rupture front during an earthquake (e.g., Aki, 1979). Nonetheless, major earthquakes may involve the simultaneous rupture of multiple, adjacent fault segments, as suggested by the large variability of stress drop observed in measurements of fault slip and

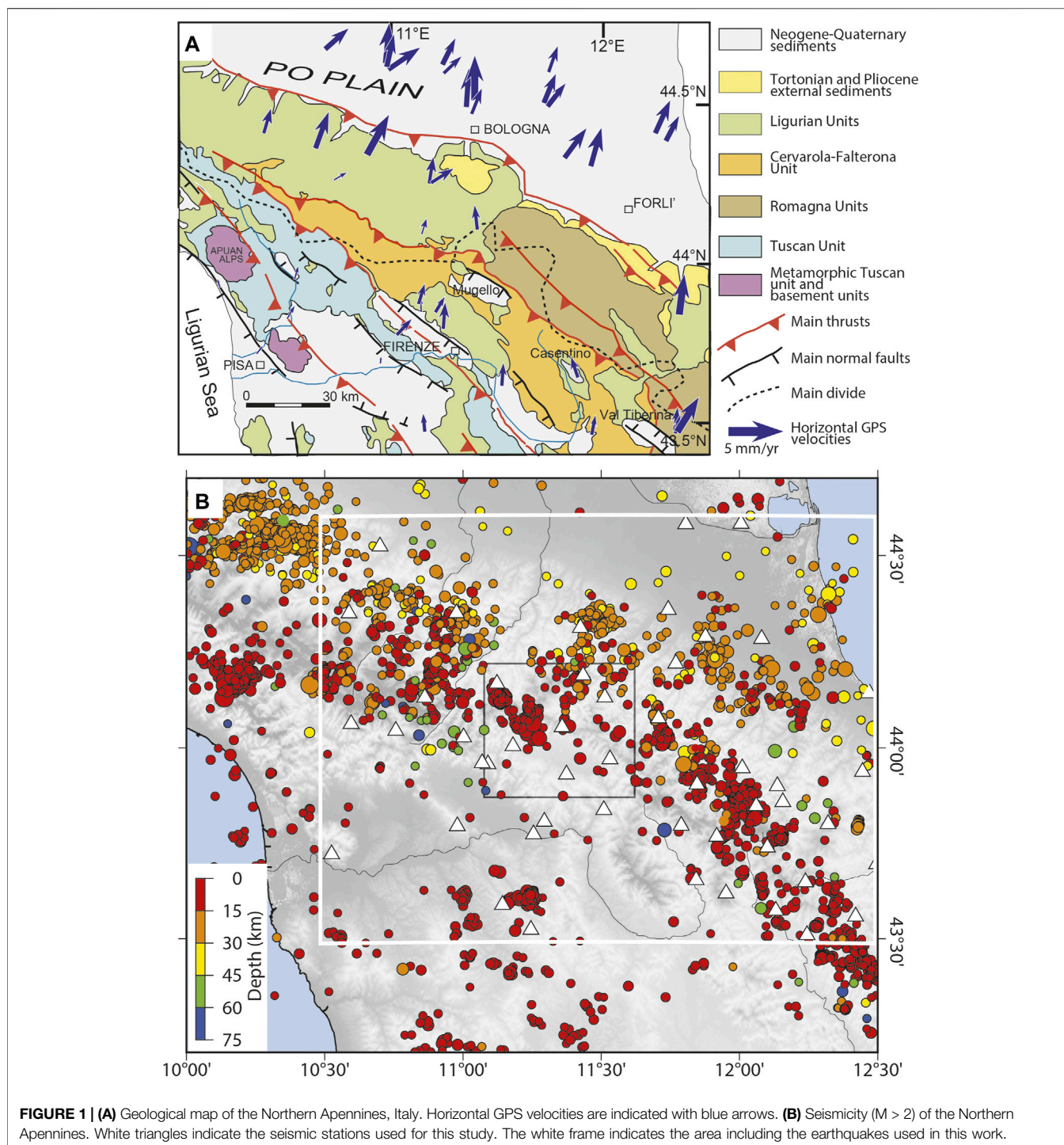


FIGURE 1 | (A) Geological map of the Northern Apennines, Italy. Horizontal GPS velocities are indicated with blue arrows. **(B)** Seismicity ($M > 2$) of the Northern Apennines. White triangles indicate the seismic stations used for this study. The white frame indicates the area including the earthquakes used in this work.

length (e.g., Manighetti et al., 2007). On the other hand, either static or dynamic stresses generated by an earthquake may concentrate at a barrier, which would thus become the locus of rupture nucleation for a subsequent earthquake (e.g., Pizzi et al., 2017). The identification of individual seismogenic segments that will likely fail during a single earthquake thus constitutes valuable constraints for the reliable assessment of seismic hazard, since it permits to bound the sites where rupture

initiates and terminates, the size of individual fault segments, and hence their maximum expected magnitude (e.g., Crone, 1991).

Located in the hinterland sector of the Northern Apennines (Italy), the intermontane Mugello Basin is a relevant seismogenic area, where earthquakes up to $M_w = 6.4$ have occurred in historical times (Rovida et al., 2020; Rovida et al., 2021); the proximity to densely-urbanized areas, and the cultural heritage in the nearby (~30 km) city of Florence, makes an improved

assessment of seismic hazard important. Over recent times, the region has been characterized by moderate seismicity. The most noticeable activity is represented by four seismic sequences during 2008–2019, with moment magnitudes M_w in the (4.2–4.5) range. The accurate analysis of those sequences may help to constrain location, geometry and size of the principal seismogenic sources in the area.

Following these arguments, this study has the main goal of identifying the active fault segments responsible for the recent seismicity in the Mugello area, and to investigate the possible interaction between those segments. This objective is pursued through 1) the definition of an integrated, high-resolution catalog of instrumental seismicity spanning the 2005–2019 time frame; 2) the accurate relocation of the target sequences, which permits identifying location and extent of individual seismogenic faults, and 3) the estimates of both static and dynamic stresses caused by the principal shocks of each seismic sequence. These results are finally discussed with reference to possible mechanisms of stress transfer and mutual interaction between the fault portions activated during the distinct sequences.

Geologic and Seismotectonic Background

The Northern Apennines fold-and-thrust belt have been developing since the Late Cretaceous following the closure of the Ligurian-Piedmontese ocean, intervening between the Europe and Adria plates (Marroni et al., 2017, and references therein). Currently, the Northern Apennines chain is composed of a complex nappe pile in which the uppermost tectonic units are the ocean-derived Ligurian Units (Jurassic-Eocene), overthrusting the Tuscan and Romagna Units (Triassic-Miocene) deposited on the thinned continental passive margin of the Adria Plate (Bonini et al., 2014, and references therein; **Figure 1A**).

The polyphase compressive tectonics which gave rise to the current fold and thrust belt continued until recent times, as suggested by recent out-of-sequence thrusting and reactivation of older thrusts (Boccaletti and Sani, 1998; Finetti et al., 2005; Bonini et al., 2014), and is still ongoing in the external sector of the chain (i.e., Po Plain) as the compressive seismic activity demonstrates (e.g., Maestrelli et al., 2018, and references therein). However, along the main Apennine divide the stress field is currently extensional, with a roughly NE-SW-oriented minimum stress axis (σ_3), as suggested by focal mechanisms (Pondrelli et al., 2002; Chiarabba et al., 2005; Pondrelli et al., 2006; Chiarabba et al., 2015) and by well developed normal fault systems, superimposed on previous compressive structures (Sani et al., 2009; Bonini et al., 2016; Sani et al., 2016, and reference therein).

The belt of the outermost hinterland intermontane Tuscan basins (Mugello, Casentino, Val Tiberina, **Figure 1A**), located near the main divide, is crucial for assessing the active tectonics and the related seismic hazard of the Northern Apennines. The Mugello is one of the more active areas of this belt and its seismicity shows a high variability in terms of intensity, depth, and kinematics (Bonini et al., 2016; **Figure 1B**). The Mugello Basin is inferred to have developed in Early Pleistocene under a compressive regime

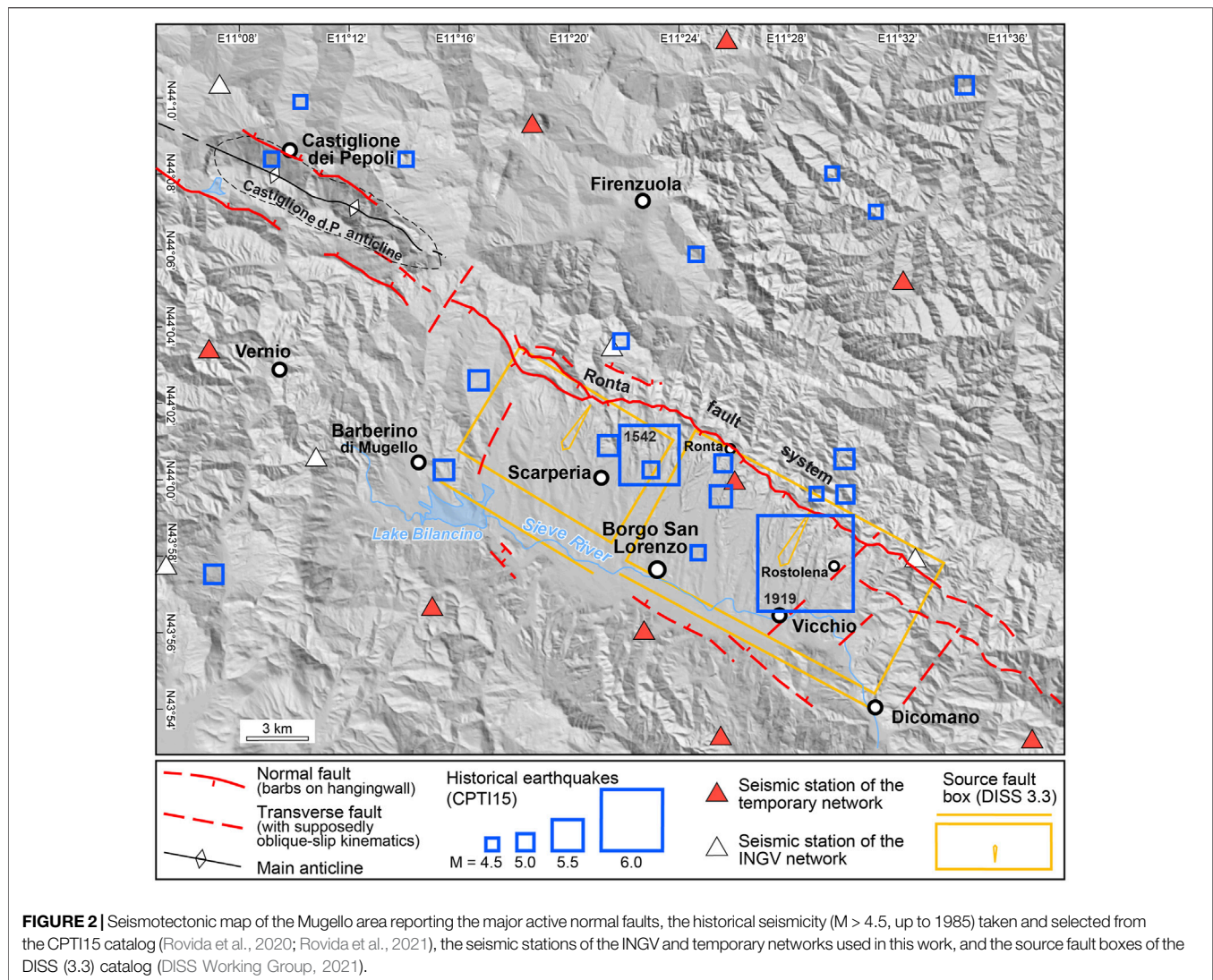
and was later affected by normal faults as the compressive regime ceased around the Early-Middle Pleistocene transition (Sani et al., 2009).

The study area is characterized by a medium intensity seismicity with historical earthquakes with highest macroseismic magnitude of $M_w = 6.02$ (1542) and $M_w = 6.38$ (1919) (Rovida et al., 2020; Rovida et al., 2021). A large SSW-dipping normal fault system, referred to as “Ronta fault system,” (RFS hereinafter) affects the pre-basin substratum mostly made of Miocene sandstones, and delimits the northeastern basin margin (Sani et al., 2009; **Figure 2**). This fault system is ~25–30 km long and displays remarkable morphostructural evidence (Sani et al., 2009; Bonini et al., 2016). Fault-slip data indicate a mainly dip-slip normal kinematics (average rake = -85°) and an average slip-rate of 0.16–0.37 mm/year has been estimated (Sani et al., 2009; Bonini et al., 2016).

The southwestern margin of the basin is affected by a system of NE-dipping antithetic normal faults, whose morphologic expression is not well pronounced (Benvenuti and Papini, 1997; Sani et al., 2009). However, it is believed to control the asymmetric location of the Sieve River on this side of the basin (Benvenuti and Papini, 1997), and previous studies locate the basin master fault along this margin (Martini and Sagri, 1993), which would be connected to the regional NE dipping low-angle Etrurian normal fault system (Buncio et al., 2000). The DISS Working Group (2021) catalog follows this interpretation and subdivides the fault system into a north-western and south-eastern segment, interpreted to have caused the earthquakes of 1542 and 1919, respectively (Basili et al., 2008). Transverse faults at the north-western and south-eastern basin margins might represent other potentially active structures (Delle Donne, 2005).

During the seismic event of 1919, coseismic east-west-trending fractures affecting the ground surface were observed in the central-eastern part of the Mugello Basin (Sani et al., 2009). Moreover, liquefaction phenomena are reported nearby the Sieve River (Galli and Meloni, 1993). Unfortunately, the rough location of these deformation features does not allow identifying the source fault of that earthquake. The distribution of the sites with highest damage may suggest that a transverse fault may have also been activated by the 1919 event (Delle Donne, 2005; Sani et al., 2009). Based on length, lateral continuity, and its clear morphological evidence, the RFS could be considered the most likely source of the biggest earthquakes that hit the Mugello area, including the 1919 event (Bonini et al., 2016).

Following that destructive earthquake, the area has been affected by weak seismicity, except for short-duration seismicity bursts characterized by a typical mainshock-aftershock sequence, and maximum magnitudes between 4 and 4.5. The most recent of these sequences occurred in 2008 ($M_w = 4.5$), 2009 ($M_w = 4.2$), 2015 ($M_w = 4.3$). This latter sequence, which occurred to the NW tip of the area of study and externally to the basin, was then followed by a minor sequence in 2017 located further NW of the 2015 cluster. The most recent sequence occurred in 2019 ($M_w = 4.5$), at the NW margin of the basin. In our research all these seismic sequences



have been relocated, allowing a better definition of orientation and dip of the causative fault segments. Particular attention is dedicated to the 2019 sequence, which was also recorded by the dense, temporary, local seismic network.

DATA

As for the rest of the Italian territory, the study area is monitored by the Italian Seismic Network (ISN), managed by the INGV-Istituto Nazionale di Geofisica e Vulcanologia (INGV Seismological Data Centre, 2006). By mid 2005, The ISN underwent a major technological upgrade, which implied a significant improvement of catalog completeness and data quality. Consequently, this study focuses on the January 2005–December 2020 time interval, during which the ISN offered the best instrumental coverage. We used the catalog produced by INGV (ISIDe Working Group, 2007) and extracted 10,094 events

located within a box of corners [43.85 N, 11.05 E] [44.20 N, 11.60 E]. For these earthquakes, we used the P- and S-wave arrival times determined manually by expert seismologists at 47 ISN seismic stations positioned in a wider region of corners [43.5 N, 10.5 E] [44.6 N, 12.5 E]. The study area is also monitored through a local network, operated by the PARSEC not-for-profit organization (<http://www.csn.prato.it/>; last accessed January 2022). From that network, we obtained hypocentral parameters and phase arrival times for 5,741 earthquakes that occurred during the time period June 2005–June 2019. From the INGV and PARSEC data sets we generated a single list of phase arrival times by merging those hypocentral solutions whose origin times differed by less than 5 s. Finally, we used data recorded by a dense temporary network composed of nine stations that we operated during the June 2019–May 2021 time span near the Mugello Basin (Bruni et al., 2019). From these stations, we used manual picks from a set of 287 catalogued earthquakes associated with the 2019 sequence (see below).

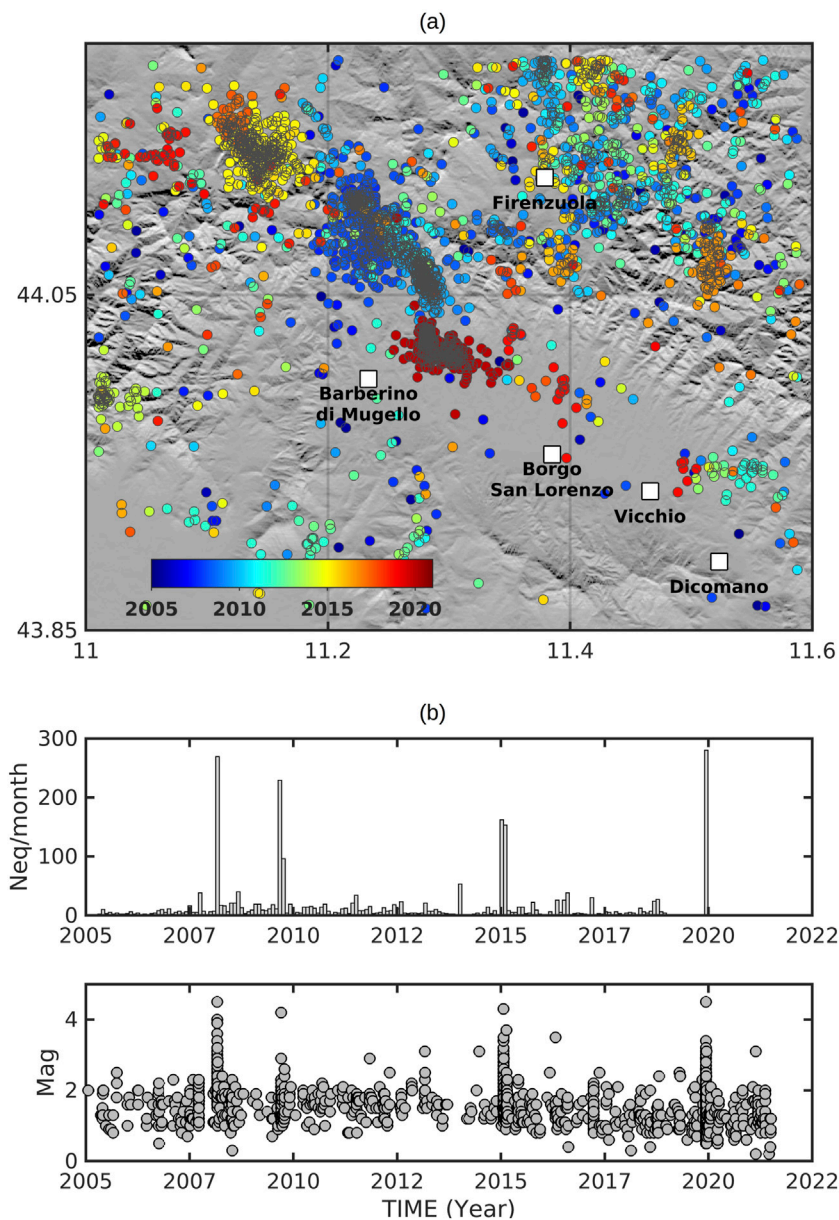


FIGURE 3 | (A) Epicentral locations from the integrated catalog. Colors scale with the origin time, according to the colorbar at the bottom. Panels in **(B)** illustrate the weekly earthquake rate and magnitudes, respectively.

METHODS

Preliminary Locations

Phase arrival times from the integrated catalog were inverted using NonLinLoc (Lomax et al., 2009), a non-linear, probabilistic procedure based on the original work of Tarantola and Valette, (1981). Theoretical travel times were calculated in reciprocal geometry using a finite-difference scheme, applied to the minimum-misfit 1D seismic velocity model derived by Piccinini et al. (2014) for the same area from inversion of local earthquakes. The resulting catalog amounts to 11,234 locations, obtained by inverting at least six wave arrival times,

with a minimum of 2 S-wave phases. Within the study area, most hypocenters are distributed according to four main spatial and temporal clusters, which occurred in March 2008 September 2009, January 2015 and December 2019 (**Figure 3**). For all these sequences, the mainshocks had similar magnitudes, spanning the range $M_w = (4.2-4.5)$.

Double Difference Relocation and Moment Tensor Solutions

Earthquakes are then relocated using HypoDD, a computer code which implements the double-difference (DD) algorithm of

Waldhauser and Ellsworth (2000). The DD technique exploits the similarity of ray paths between the source and a common station when the hypocentral separation between two earthquakes is small with respect to the event-station distance and the wavelength of velocity heterogeneity. This approach permits to reduce systematic errors related to the prediction of travel times in poorly known velocity structures, and hence to achieve more focused images of hypocenter clustering. We only consider earthquakes included in a box of corners [43.95 N, 11.05 E] [44.30 N, 11.80 E], and located with a minimum of 12 phases.

Source mechanisms for the most relevant earthquakes are taken from the Time Domain Moment Tensor (TDMT) catalog (Scognamiglio et al., 2006), which reports the solutions obtained using the full-waveform moment-tensor inversion of Dreger and Helmberger (1993), as described in Scognamiglio et al. (2009).

Evaluation of Static and Dynamic Stress Changes

Stress relieved during an earthquake can influence the stress state on faults surrounding the ruptured fault (e.g., Stein, 1999; Kilb et al., 2002; Kilb, 2003; Hill and Prejean, 2007; King and Devès, 2015). We thus evaluate the potential role of dynamic and static stress changes on the sequence of small to moderate earthquakes that struck the northern margin of the Mugello basin in 2008–2019.

Static stresses can permanently modify the stress in the crust around the fault rupture, and attenuate away from it as $1/R^3$, R being the epicentral distance (Aki and Richards, 1980). Consequently, stress acting on faults nearby the earthquake can be changed depending on the position, geometry and rake of the considered receiver fault. Coulomb stress changes imparted by a mainshock were computed in a homogeneous elastic half-space and resolved on the fault rupture associated with the subsequent mainshock using available source fault models (Supplementary Tables S1, S2) and the Coulomb 3.3 software (Lin and Stein, 2004; Toda et al., 2005). Coulomb stress changes (ΔCFF) are defined as $\Delta CFF = \Delta\tau + \mu' \Delta\sigma_n$, where $\Delta\tau$ is the shear stress change (positive in the direction of slippage), $\Delta\sigma_n$ is the fault-normal stress change (positive for fault unclamping), and μ' is the apparent friction, which is an approximation of fault properties (e.g., static friction, pore-pressure conditions). Failure is encouraged if ΔCFF is positive, whereby a fault will fail if the applied stress increments exceed a stress threshold specific for the fault. Increased shear stress and fault unclamping are normally considered favorable conditions for failure. Fault failure is instead hindered if ΔCFF is negative, which occurs for decreased shear stress on faults and if the fault is clamped.

Dynamic stresses, σ_{pd} , produced by passing seismic waves decay much slower with epicentral distance (as $\sim 1/R^2$ or $\sim 1/R^{1.5}$; Hill and Prejean, 2007), and can thus trigger earthquakes distantly (Hill et al., 1993; Kilb et al., 2002; Brodsky et al., 2003). Most observations indicate that dynamic triggering occurs in concomitance of the transit of the largest-amplitude seismic arrivals, such as the Rayleigh waves (e.g., Hill and Prejean, 2007). However, other studies suggest that such transient

stress changes may alter the properties of a pre-existing fault, accelerating its evolution toward failure (Parsons, 2005). In that case, the triggering may be delayed by up to several years (e.g., Kilb, 2003).

The effects of the dynamic stresses are evaluated by estimating, for each mainshock, the peak ground velocity (PGV) at the faults which ruptured subsequently. PGV is derived from the ground motion predictive equation of Bindi et al. (2011), which is routinely used for the production of shake maps (Michellini et al., 2020; Supplementary Figure S3). This analysis admittedly involves some degree of uncertainty related to the simplifying approximation that PGV predicted at the earth surface is similar to that at hypocentral depth. Nevertheless, the decrease with depth of amplitude and strain of surface seismic waves will be balanced at some extent by the tendency of elastic moduli to increase with depth (Hill and Prejean, 2007). Peak dynamic stresses (σ_{pd}) are derived from PGV following the relationship (Hill et al., 1993; Hill and Prejean, 2007; Fan et al., 2021):

$$\sigma_{pd} = PGV G \beta^{-1} \quad (1)$$

where G is the shear modulus and β is the average S-wave velocity, here taken equal to 32 GPa and 3,200 m/s, respectively.

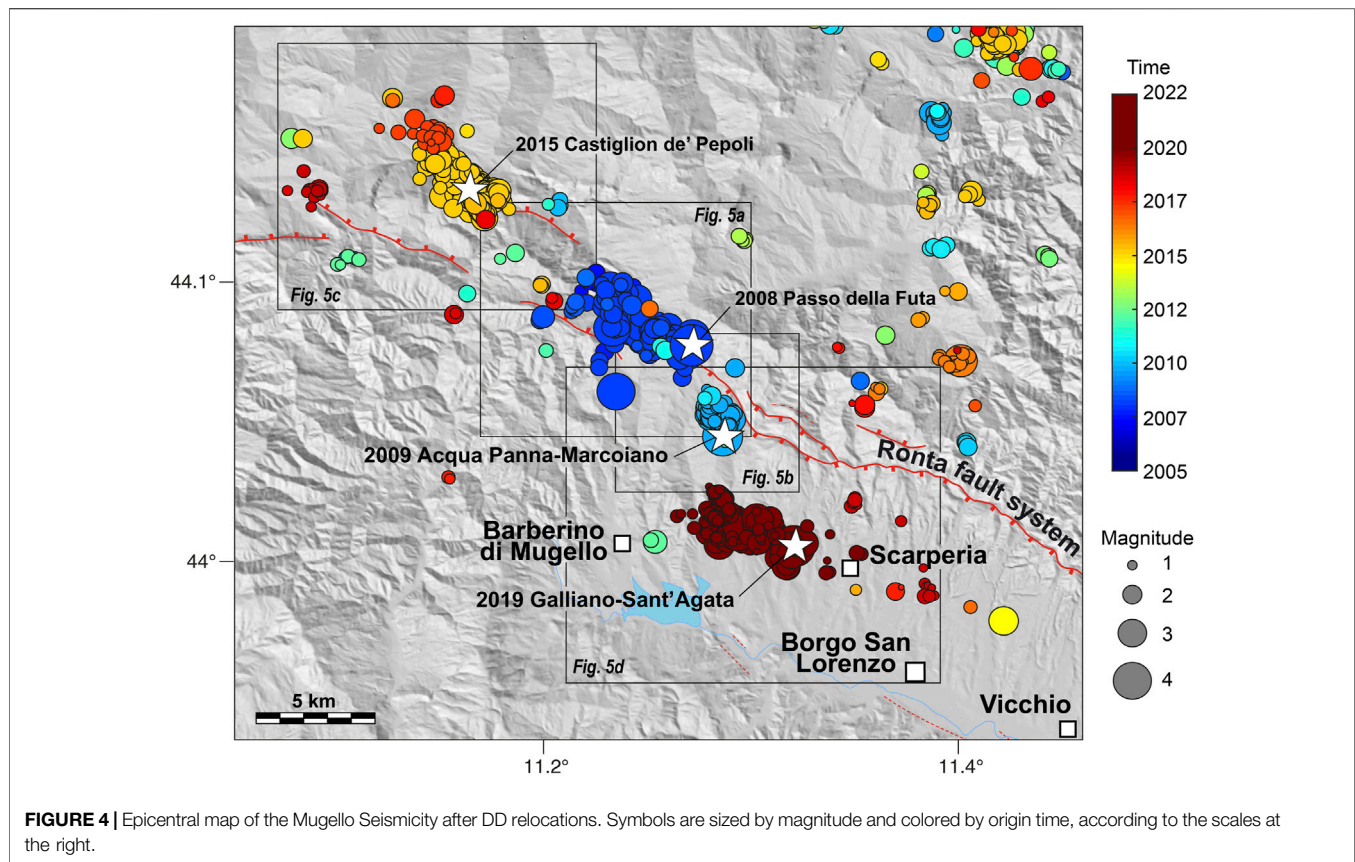
RESULTS

The 1329 DD solutions clearly show the spatial clustering of the four sequences which affected the study area in 2008, 2009, 2015–2017, and 2019 (Figure 4). Overall, these clusters align along NW-SE-trending structures bordering the northern margin of the basin, and extend beyond its NW tip. In all four episodes, the mainshock occurs at the very early stage of the sequence, and the following aftershocks decay rapidly, roughly abiding Omori's law (see Supplementary Figure S1).

Figure 5, panels 1) through 8) illustrate the detail of the individual sequences, together with the moment tensor solution of the respective mainshocks as reported by the TDMT catalog (Scognamiglio et al., 2006). For each sequence, the plane best fitting hypocentral data is derived from an orthonormal regression via Principal Component Analysis (PCA) (see Supplementary Figure S2, Table S1). The vertical cross-sections shown in panels (b,d,f,h) are taken along directions perpendicular to the strike of those planes, and also report the projection of the available TDMT solution(s).

2008 Passo della Futa—Hypocenters from the 2008 sequence are distributed in the 7–12 km depth range along a steep NNE-dipping planar structure (Figures 5A,B), consistent with the previous findings by Piccinini et al. (2014) and Bonini et al. (2016). The mainshock occurred on March 1, 2008, at 07:43 UTC, with moment magnitude $M_w = 4.5$. It was rapidly followed by two other shocks at 08:43 and 10:43, with M_w equal to 4.0 and 3.9, respectively.

2009 Acqua Panna-Marcoiano—The 2009 sequence had a mainshock of $M_w = 4.2$ that occurred on September 14, 2009, and hit the NW margin of the Mugello Basin. The hypocenters' distribution of this sequence delineates a SSW-dipping normal



fault ascribable to the RFS (**Figures 5C,D**), consistent with the previous studies by Piccinini et al. (2014) and Bonini et al. (2016).

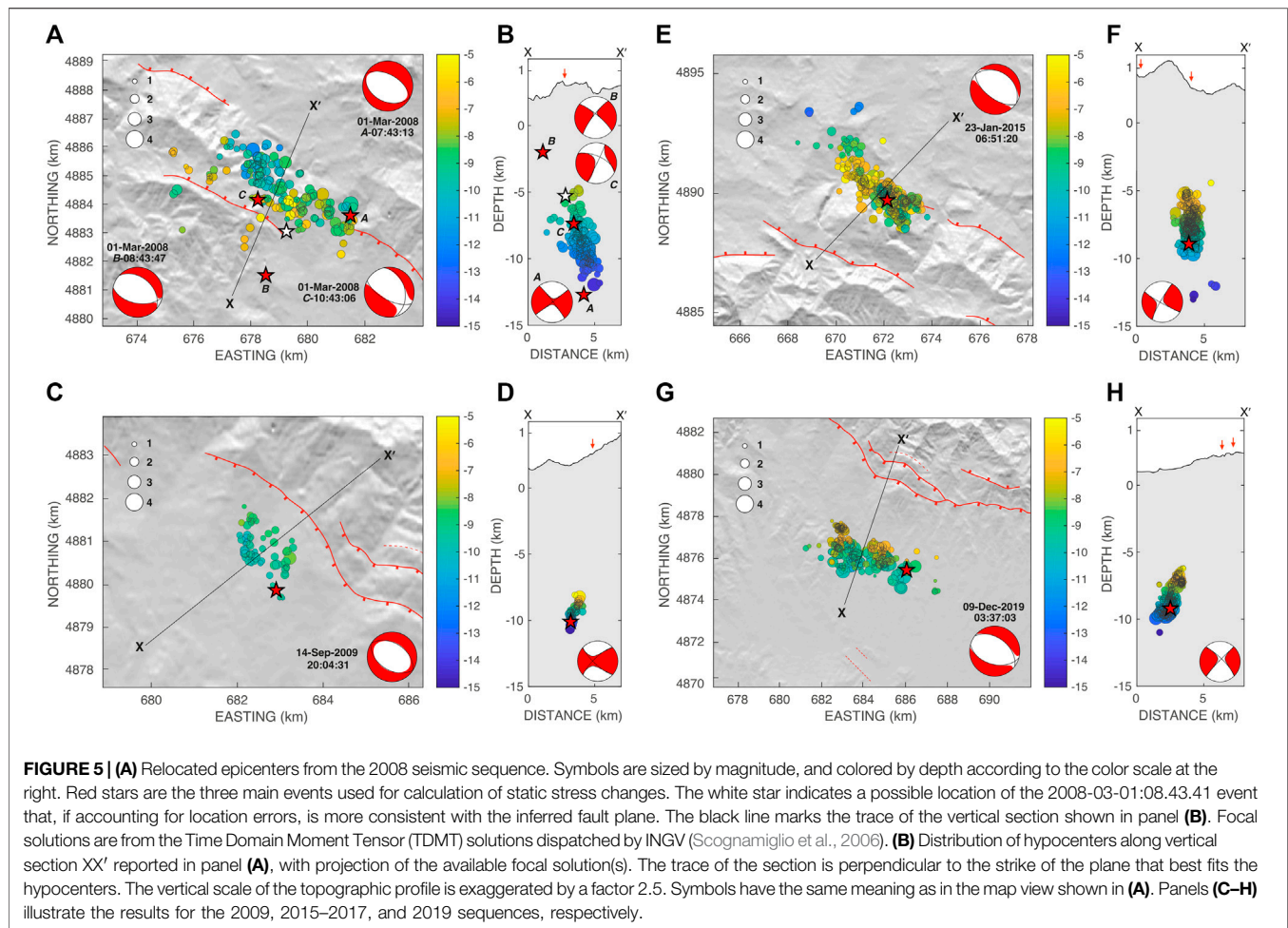
2015–2017 Castiglion de' Pepoli—The mainshock of this sequence occurred on January 23, 2015, with a M_w of 4.3. The following aftershocks define a sub-vertical cluster trending NW-SE, and hypocentral depths span the 5–10 km depth interval (**Figures 5E,F**). Seismicity then renewed during 2017, with a small cluster located at the NW tip of the 2015 structure, at depths of around 9 km (**Figures 5E,F**).

2019 Galliano-Sant'Agata—The mainshock of this sequence occurred on December 9, 2019, at 03:37 UTC with $M_w = 4.5$. The DD relocation delineates a NW-SE-trending, SW-dipping planar structure extending over the 6–11 km depth interval (**Figures 5G,H**). This geometry is in agreement with the TDMT solution of the mainshock, which indicates a normal fault striking $N105^\circ E$ and dipping about 45° (see **Figures 5G,H**).

The structures delineated by hypocentral alignment are oriented consistently with the corresponding TDMT solution(s), with maximum angular discrepancies in either strike or dip angles on the order of 20° . The most striking mismatch between the two estimates is associated with the 2015–2017 Castiglion de' Pepoli sequence. In that case, relocations indicate a sub-vertical plane steeply ($\sim 85^\circ$) dipping NE, while TDMT results point to a plane SW-dipping with an inclination of 60° . Several factors may be invoked to explain such disagreement. The first is that TDMT estimates are more sensitive

to unmodeled velocity heterogeneities than DD locations. Second, TDMT solutions were obtained using INGV's epicentral coordinates which, in some cases, differ by up to 3–4 km from those derived in our relocations. Finally, several of the TDMT solutions exhibit significant non-double-couple components, an occurrence that in principle could be attributed to non-planar fault surfaces and/or the simultaneous failure of distinct fault patches oriented differently. However, considering the dimension of the faults at play, it is more likely that those non-DC components are associated with a lack of constraints due to poor station coverage (e.g., Rösler and Stein, 2022). Following these arguments, we deem that the fault planes imaged through hypocentral fitting are more constrained than those derived from the TDMT solution.

Coulomb stress changes associated with the 2008–2019 mainshocks are predictably small. In particular, the ΔCFF produced by the 3 (Passo della Futa) earthquakes of March 01, 2008 caused a stress increase of nearly 5 kPa on the hypocenter of the 2009 Acqua Panna-Marcoiano earthquake (**Figure 6A**; **Supplementary Table S2**). Instead, the 2008 and 2009 earthquakes produced a feeble ΔCFF increment of just 1 kPa on the 2019 Galliano-Sant'Agata fault rupture, and an exceedingly small ΔCFF at the location of the January 23, 2015 (Castiglion de' Pepoli) earthquake (**Figure 6B**; **Supplementary Table S2**). The small magnitude of stress changes suggests that there is little static stress interaction



among the seismic sources. There is instead a good correlation between static stress changes and aftershocks, the latter being dominantly located in the positive lobes of ΔCFF produced by a mainshock (e.g., red-yellow areas in **Figures 6A–C**).

Static stress changes discussed above have been derived using mainshock locations and geometric fault parameters (except rake) derived from DD relocations and PCA fitting. In order to verify the dependence of those estimates on fault parameters, we also repeated the calculations using fault parameters derived from TDMT solutions. The results, reported in **Supplementary Table S3**, are of the same order of magnitude of those derived previously, leaving the main conclusions basically unchanged.

Dynamic stress changes are evaluated for the six independent pairs of mainshocks, whose inter-hypocenter distances range between ~ 4 km (2009–2019 pair) and 21 km (2015–2019 pair). The highest and lowest PGV estimates are those of the 2008–2009 and 2015–2019 pairs, amounting to 3×10^{-2} m/s and 5×10^{-3} m/s, respectively. As a consequence of the large uncertainties in the prediction of PGVs, peak dynamic stresses have a large variability (**Supplementary Tables S3, S4**). The largest dynamic stresses are those associated with the 2008–2009 and 2009–2019 pairs that, taking uncertainties into account, amount to more than 0.5 GPa (**Figure 7**).

DISCUSSION

Active Structures and Seismotectonic Implications

The high-resolution relocation of seismic data clearly indicates that the four main sequences that affected the study area during the past 13 years were associated with the subsequent activation of adjacent segments of a larger fault system bordering the NE sector of the Mugello Basin and adjoining areas. In particular, the 2019 and 2009 sequences are clearly correlated with two segments of the RFS. Both focal mechanisms and the SW-dipping fault planes imaged by the hypocenter clusters correlate remarkably well with the fault geometry delineated by the surface geology (Sani et al., 2009; Bonini et al., 2016).

The 2008 and 2015–2017 sequences are located externally to the basin, but in continuity with the RFS. The 2008 sequence is related to a NE-dipping plane, in agreement also with what reported by Piccinini et al. (2014), and Bonini et al. (2016). The fault segment activated during the 2015 Castiglion de' Pepoli sequence is steeply dipping toward NE, and it is likely related to a system of normal faults affecting the Castiglion de' Pepoli anticline (**Figures 2, 5**). The geometrical relationships between the RFS and the NE-dipping fault planes are unclear, even though the differences in

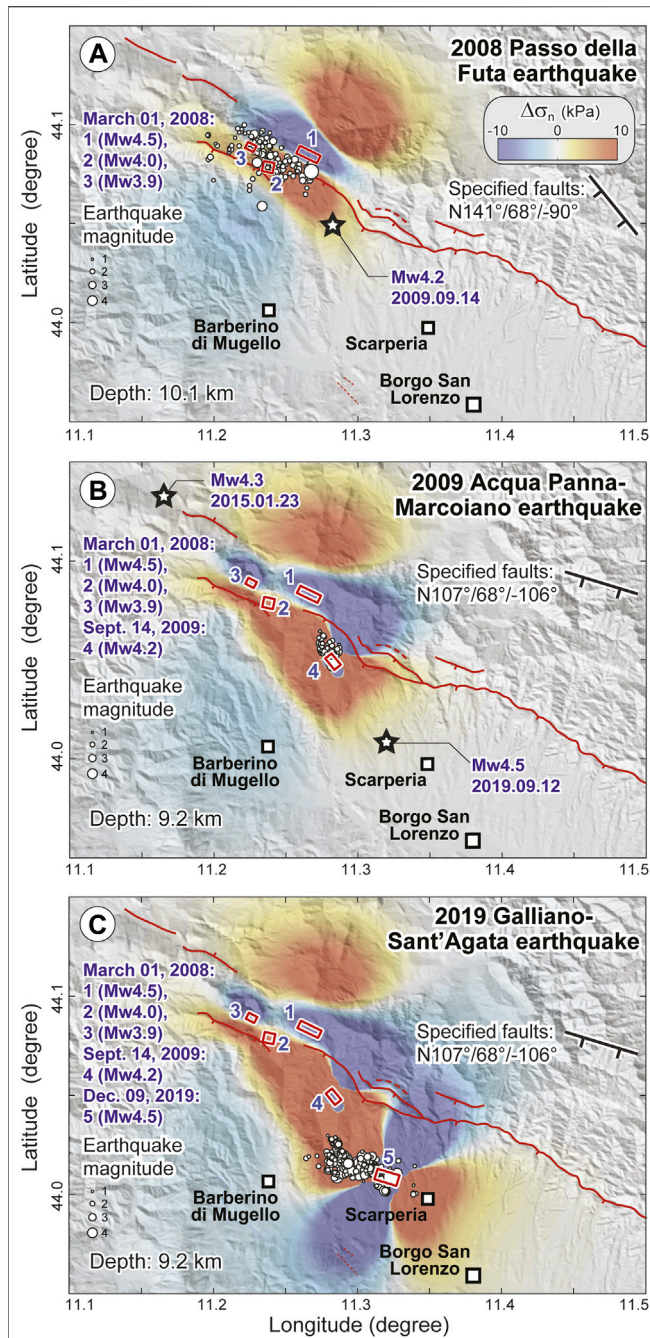


FIGURE 6 | Coulomb stress changes (ΔCFF) produced by normal faults in the north-eastern margin of the Mugello Basin. ΔCFF (red-yellow and blue areas indicate stress rise and stress drop, respectively) are reported in subsequent time windows and are computed on receiver faults with geometry and rake of the subsequent rupture (for instance, the ΔCFF produced by the 2008 earthquakes are computed on the fault that ruptured in 2009). Coulomb stress changes are shown as cumulative effects produced by multiple fault ruptures: **(A)** 2008 Passo della Futa earthquakes. **(B)** 2009 Acqua Panna-Marcoiano earthquake plus 2008 earthquakes. **(C)** 2019 Galliano-Sant'Agata earthquake plus 2008 and 2009 earthquakes. The open white circles indicate relocated epicenters of the aftershocks of a given mainshock (aftershocks are as those reported in **Figure 5**).

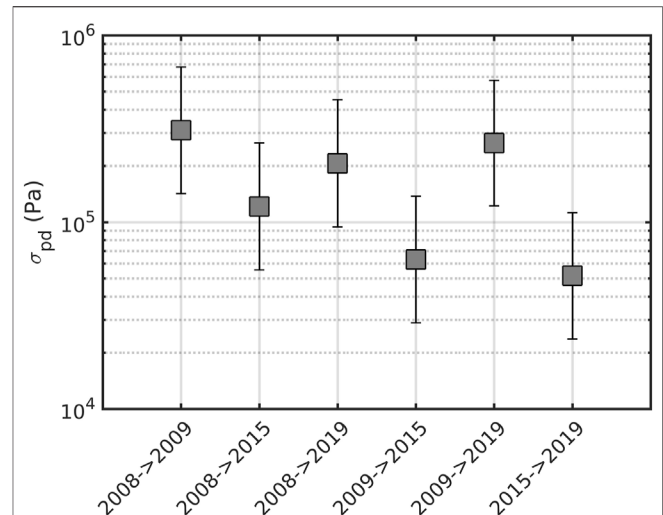


FIGURE 7 | Estimates of the peak dynamic stress that each mainshock produced at the hypocentral location(s) of the mainshock(s) of the subsequent sequence(s). As an example, the “2008–2019” datum indicates the peak stress generated by the 2008 mainshock at the hypocenter of the 2019 mainshock. Error bars derive from the uncertainties in PGV predictions (**Supplementary Figure S3**).

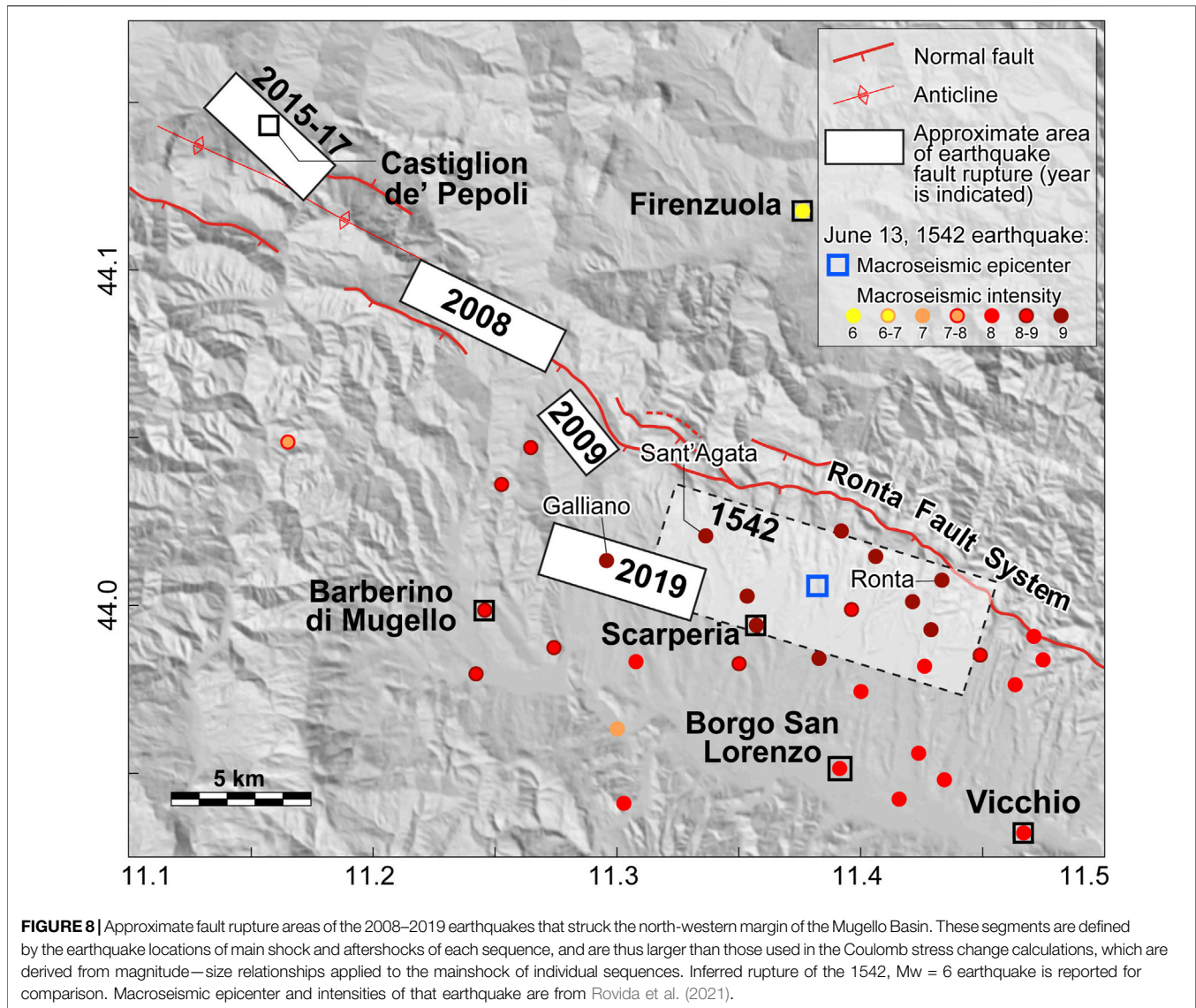
fault geometry and morphological characteristics (with the RFS being characterized by marked morphological features, and the NE-dipping fault planes being mostly blind) may suggest that they belong to distinct fault systems.

The activation of the 2009 and 2019 fault ruptures fits well with the overall distribution of historical earthquakes, which are arranged along a NW-SE-trending belt, which runs sub-parallel to the RFS, near the North-Eastern margin of the basin.

These findings have obvious implications for the regional seismotectonic setting of the study region. In particular, both geometry and depth extent of the ruptured faults are not consistent with the activity of a low-angle, NE-dipping normal fault (i.e., the Etrurian Fault System; Boncio et al., 2000; DISS Working Group, 2021) which is hypothesized to be emerging at the South-Western margin of the basin. As a matter of fact, simple geometrical considerations suggest that the rupturing depths (which are of the order of 10 km) are deeper than the prosecution at depth of such a hypothetical low-angle normal fault. Finally, this observation also rules out the possibility that the SW-dipping normal faults represent antithetic structures to the Etrurian Fault System. These findings thus challenge the ongoing activity, or even the existence of the Etrurian Fault System in the Mugello region.

Potential Seismic Triggering

The four main shocks occurred at relatively close distances and during a relatively short time span, and therefore a role of seismic triggering could potentially be involved. Nevertheless, the triggering mechanisms should explain the relatively long time intervals between the mainshocks, which occurred with delays varying between 1.5 and 10 years. Actually, identifying the



processes that control delayed activation is intricate: on the one hand, permanent static stresses can be predicted as a possible mechanism, but they are small. On the other hand, dynamic stresses are relatively large, but transient, with the triggering more than a year after the passage of the seismic waves being difficult to explain.

A triggering threshold for static stress changes has been generally set at 10 kPa (Stein, 1999), while dynamic stresses as small as 0.1–5 kPa are reported to have triggered seismicity (e.g., Brodsky and Prejean 2005; van der Elst and Brodsky 2010; Saccorotti et al., 2013). If such small stress thresholds can be also valid for static stress changes, then the consideration that some faults (before rupturing) experienced similar small stress magnitudes raises the possibility that static stresses may have played a role in the triggering (especially for the 2009 Acqua Panna-Marcoiano earthquake, for which the highest static stress changes are estimated). Notwithstanding the modest magnitude,

Coulomb stress changes have loaded all the considered fault ruptures, and if Coulomb stress changes produced by any earthquake are cumulative, even small stress increases may “advance the clock” of the next earthquake, although it is currently unknown whether the considered faults exhibit such a sensitivity.

Another important issue regards the role of dynamic stresses in delayed triggering. Although dynamic stresses are transient, they can occasionally be converted into permanent deformation, for instance when seismic waves breach hydraulic barriers separating different fluid compartments (e.g., Manga et al., 2009). In addition, rapid fluid flow induced by seismic waves can remove temporary barriers within fractures and faults leading to pore pressure redistribution (Brodsky et al., 2003). Accordingly, Kilb (2003) envisaged that peak dynamic stresses induced by the 1992 $M_{7.3}$ Landers earthquake would have played a role in triggering the next 1999 $M_{7.1}$ Hector Mine earthquake.

In particular, such a delayed triggering has been related to variations in the properties of fault zones (e.g., changes in friction and pore fluid pressures) induced by dynamic stress change oscillations (see also Parsons, 2005), whereby faults become weaker and thus more prone to rupture.

The role of dynamic shaking in delayed triggering could be evaluated considering the tensile strength of rock anisotropies that are conceivably common in fault zones. In this regard, the peak dynamic stresses on the order of 500 kPa estimated at some epicentral locations of the 2008–2019 Mugello seismic sequences (Figure 7), are included into the range of tensile strengths of rock anisotropies (i.e., mineral veins, schistosity planes, joints and faults), as experimentally determined by Shang et al. (2016). Therefore, suitably oriented dynamic stresses could potentially breach some of these discontinuities, opening routes for the escape of fluids from pressurized compartments or altering the scale length of the frictional contacts.

Applying these lessons to the north-eastern margin of the Mugello Basin, we raise the possibility that seismic perturbations would have played some role in triggering some of the mainshocks of the 2008–2019 sequence, although with modalities that may differ depending on the case (see Figures 7, 8, and Supplementary Tables S2, S3).

On the basis of the magnitude of static and dynamic stress changes, the 2009 Acqua Panna-Marcoiano earthquake was seemingly triggered by a combination of both types of stress changes. Static stresses are exceedingly small for the 2015 earthquake, and thus dynamic stress changes can be conceivably envisaged as the only potential driver. More ambiguous is the attribution of the 2019 Galliano-Sant'Agata earthquake, which occurred 10 years after the closest mainshock of the sequence (i.e., the 2009 Acqua Panna-Marcoiano earthquake). Also in this case dynamic stresses are much larger than static stresses (cf. Figure 7 and Supplementary Tables S2–S4), and so the actual role of the very small positive Coulomb stress change (i.e., 1 kPa) is uncertain.

Admittedly, the evidence for the seismic triggering is not solid. Nevertheless, the 4 $M > 4$ earthquakes clustered over a relatively short time interval (approx. 11 years), marking a significant increase of the seismicity rate with respect to the previous decades (see Supplementary Figure S4). In this respect, it is also worth noting that for that same magnitude range, the seismic catalog of the area is assumed to be complete since at least the second half of the 19th century (Visini et al., 2022). This spatial and temporal clustering may thus suggest that the ruptured faults were relatively close to failure. If so, this condition would be consistent with the hypothesis that earthquake-related stresses have played some role in the triggering of some 2009–2019 mainshocks.

Relationships With Large Historical Earthquakes

The north-eastern margin of the Mugello Basin has experienced large historical earthquakes, particularly the 1542, $M_w = 6$ Scarperia earthquake and the $M_w \approx 6.4$ 1919 Vicchio earthquake (Rovida et al., 2021; Figure 1). Such large

earthquakes have been correlated to the activity of the RFS (Bonini et al., 2016; this study). The overall framework resulting from the present analysis clearly points to the activation of distinct segments of the RFS. In particular, earthquake ruptures of 2009 and 2019 have been correlated to two RFS segments located in proximity of the macroseismic epicenter of 1542. Fault scaling relationships indicate that the 1542 rupture had a length of ca. 12 km and a width of ca. 8.5 km (Wells and Coppersmith, 1994). Notwithstanding the uncertainties of macroseismic epicentral locations, the fault rupture area caused by the 1542 earthquake conceivably includes the RFS segment activated during the 2019 sequence. This hypothesis is also supported by the observation that the highest macroseismic intensity of the 1542 earthquake ($MCS = 9$) has been documented at localities sited over the ruptured area of 2019 (e.g., Sant'Agata and Galliano; Figure 8). The evidence points towards the 1542 earthquake rupturing at least part, if not all the, the fault segment that ruptured in 2019. Less clear is the spatial correlation between the 1542 earthquake and the RFS fault segment that ruptured in 2009.

The four seismic sequences that we have relocated define similar fault segment geometries (Figure 8), with typical lengths and widths spanning the (2, 6)km range. In some cases, especially the 2009 and 2019 sequences, the subsurface fault segment matches in length, position and orientation to the associated surface expression of the RFS. This, coupled with the interpretation that the western end of the 1542 earthquake likely included the fault segment that ruptured in 2019, has the implication that the 1542 event involved the failure of multiple (likely two or 3) segments of the RFS.

CONCLUDING REMARKS

The results from this study lead to the following main conclusions:

- 1) The seismic sequences which affected the Mugello area in 2008–2019 were caused by distinct fault segments, two of which belong to the RFS bordering the NE margin of the basin (namely, the 2009 and 2019 ones), while the remaining two (2008 and 2015–2017) pertain to distinct, NE-dipping steep faults.
- 2) The spatial and temporal clustering of the four sequences, which interrupted a relatively long period of seismic quiescence, suggest some interaction among the segments which ruptured in individual sequences. A different contribution of dynamic and static stress changes is inferred for the possibly triggered fault ruptures.
- 3) Our findings reveal that fault segments of the RFS bordering the basin can fail individually, as for the 2019 episode, or earthquake rupture can propagate across segment boundaries to rupture multiple fault segments producing larger magnitude earthquakes. Whereas the 1542, $M_w = 6$ Mugello earthquake was seemingly produced by the activation of two or more adjacent

segments, the observation that there are no large historical earthquakes northwest of the Mugello Basin may suggest that the fault segments in this area tend to rupture individually (e.g., the 2008 and 2015–2017 sequences). The reasons leading to such different behaviors are conceivably depending on the mechanical coupling between contiguous fault portions, but quantitative constraints on this process are unknown so far. This issue needs further investigations, as it is crucial for assessing the seismic hazard of the region.

DATA AVAILABILITY STATEMENT

The datasets presented in this article are not readily available because they are embargoed until January 2023. The integrated parametric catalog is available upon request to the authors; requests should be directed to GS, gilberto.saccorotti@ingv.it.

AUTHOR CONTRIBUTIONS

GS, MB, GC, DK, and FS contributed to the conception and design of the study. DK provided instruments for temporary deployment from SEISUK; RB contributed to data acquisition, curation and visualization; MB, GS, and RB conducted formal analysis; FS, DK and GC supervised the work. All authors contributed to manuscript writing, revision, read, and approved the submitted version.

REFERENCES

- Aki, K. (1979). Characterization of Barriers on an Earthquake Fault. *J. Geophys. Res.* 84 (B11), 6140–6148. doi:10.1029/JB084iB11p06140
- Aki, K., and Richards, G. P. (1980). *Quantitative Seismology, Theory and Methods*. New York: W. H. Freeman, 1–932.
- Basili, R., Valensise, G., Vannoli, P., Burrato, P., Fracassi, U., Mariano, S., et al. (2008). The Database of Individual Seismogenic Sources (DISS), Version 3: Summarizing 20 Years of Research on Italy's Earthquake Geology. *Tectonophysics*. 453, 20–43. doi:10.1016/j.tecto.2007.04.014
- Benvenuti, M., and Papini, M. (1997). Depositi continentali Plio-Pleistocenici nell'area di Monte Giovi. Relazioni tra l'evoluzione idrografica e la tettonica della Valdisieve (Firenze). *Quaternario*. 10, 105–120.
- Bindi, D., Pacor, F., Luzi, L., Puglia, R., Massa, M., Ameri, G., et al. (2011). Ground Motion Prediction Equations Derived from the Italian strong Motion Database. *Bull. Earthquake Eng.* 9 (6), 1899–1920. doi:10.1007/s10518-011-9313-z
- Boccaletti, M., and Sani, F. (1998). Cover Thrust Reactivations Related to Internal Basement Involvement during Neogene-Quaternary Evolution of the Northern Apennines. *Tectonics*. 17, 112–130. doi:10.1029/97TC02067
- Boncio, P., Brozzetti, F., and Lavecchia, G. (2000). Architecture and Seismotectonics of a Regional Low-Angle normal Fault Zone in central Italy. *Tectonics*. 19 (6), 1038–1055. doi:10.1029/2000tc900023
- Bonini, M., Corti, G., Donne, D. D., Sani, F., Piccardi, L., Vannucci, G., et al. (2016). Seismic Sources and Stress Transfer Interaction Among Axial Normal Faults And External Thrust Fronts in The Northern Apennines (Italy): A Working Hypothesis Based on the 1916–1920 Time-Space

FUNDING

The facilities of SEISUK are supported by the Natural Environment Research Council (NERC) under agreement R8/H10/64. DK acknowledges support from NERC grant NE/L013932/1 and from the University of Florence funds ATEN 2019, 2020, and 2021. PhD scholarship to RB was funded by the Pegaso fellowship scheme awarded by Regione Toscana.

ACKNOWLEDGMENTS

Thoughtful comments from two reviewers greatly helped to improve the quality of the manuscript. We are sincerely grateful to Marco Capello, Damiano Biagini and Michele d'Ambrosio for their continuous effort in the installation and maintenance of the 9M seismic network. Andrea Fiaschi provided phase arrival time data from the PARSEC seismic network. Carlo Giunchi and Davide Piccinini maintained data acquisition and storage from the 9M network. *The Unione dei Comuni Valdarno e Val di Sieve* and *Unione Montana dei Comuni del Mugello* provided logistic and economic support to the project, respectively. The seismic instruments of the 9M network were loaned from SEISUK.

SUPPLEMENTARY MATERIAL

The Supplementary Material for this article can be found online at: <https://www.frontiersin.org/articles/10.3389/feart.2022.879160/full#supplementary-material>

- Cluster Of Earthquakes. *Tectonophysics*. 680, 67–89. doi:10.1016/j.tecto.2016.04.045
- Bonini, M., Sani, F., Stucchi, E. M., Moratti, G., Benvenuti, M., Menanno, G., et al. (2014). Late Miocene Shortening of the Northern Apennines Back-Arc. *J. Geodynamics*. 74, 1–31. doi:10.1016/j.jog.2013.11.002
- Brodsky, E. E., and Prejean, S. G. (2005). New Constraints on Mechanisms of Remotely Triggered Seismicity at Long Valley Caldera. *J. Geophys. Res.* 110, B04302. doi:10.1029/2004JB003211
- Brodsky, E. E., Roeloffs, E., Woodcock, D., Gall, I., and Manga, M. (2003). A Mechanism for Sustained Groundwater Pressure Changes Induced by Distant Earthquakes. *J. Geophys. Res.* 108, 2390. doi:10.1029/2002jb002321
- Bruni, R., Saccorotti, G., Keir, D., Giunchi, C., and Fiaschi, A. (2019). “Mugello Temporary Seismic Deployment [Data Set],” in *International Federation of Digital Seismograph Networks*. doi:10.7914/SN/9M_2019
- Chiarabba, C., De Gori, P., and Mele, F. M. (2015). Recent Seismicity of Italy: Active Tectonics of the central Mediterranean Region and Seismicity Rate Changes after the Mw 6.3 L'Aquila Earthquake. *Tectonophysics* 638, 82–93. doi:10.1016/j.tecto.2014.10.016
- Chiarabba, C., Jovane, L., and DiStefano, R. (2005). A New View of Italian Seismicity Using 20 Years of Instrumental Recordings. *Tectonophysics*. 395, 251–268. doi:10.1016/j.tecto.2004.09.013
- Crone, A. J., and Haller, K. M. (1991). Segmentation and the Coseismic Behavior of Basin and Range normal Faults: Examples from East-central Idaho and Southwestern Montana, U.S.A. *J. Struct. Geology*. 13 (2), 151–164. doi:10.1016/0191-8141(91)90063-O
- Delle Donne, D. (2005). *Tettonica attiva dell'Appennino Settentrionale nel settore compreso tra l'Appennino Pistoiese e l'alta Val Tiberina*. Florence, Italy: Unpublished PhD Thesis, University of Florence.
- DISS Working Group (2021). *Database of Individual Seismogenic Sources (DISS), Version 3.3.0: A Compilation of Potential Sources for Earthquakes Larger than M*

- 5.5 in Italy and Surrounding Areas. Italy: Istituto Nazionale di Geofisica e Vulcanologia INGV.
- Dreger, D. S., and HelMBERGER, D. V. (1993). Determination of Source Parameters at Regional Distances with Three-Component Sparse Network Data. *J. Geophys. Res.* 98, 8107–8125. doi:10.1029/93JB00023
- Fan, W., Barbour, A. J., Cochran, E. S., and Lin, G. (2021). Characteristics of Frequent Dynamic Triggering of Microearthquakes in Southern California. *J. Geophys. Res. Solid Earth*. 126, e2020JB020820. doi:10.1029/2020JB020820
- Finetti, I. R., Boccaletti, M., Bonini, M., Del Ben, A., Pipan, M., Prizzon, A., et al. (2005). “Lithospheric Tectono-Stratigraphic Setting of the Ligurian Sea-Northern Apennines-Adriatic Foreland from Integrated CROP Seismic Data,” in *CROP PROJECT: Deep Seismic Exploration of the Central Mediterranean and Italy, Atlases in Geosciences*. Editor I. R. Finetti (Elsevier), 1, 119–158. Chapter 8.
- Galli, P., and Meloni, F. (1993). Nuovo catalogo dei processi di liquefazione avvenuti in occasione dei terremoti storici in Italia. *Quaternario*. 6 (2), 271–292.
- Hill, D. P., Reasenberg, P. A., Michael, A., Arabaz, W. J., Beroza, G., Brumbaugh, D., et al. (1993). Seismicity Remotely Triggered by the Magnitude 7.3 Landers, California, Earthquake. *Science*. 260, 1617–1623. doi:10.1126/science.260.5114.1617
- Hill, D., and Prejean, S. (2007). “Dynamic Triggering,” in *Treatise on Geophysics Volume 4: Earthquake Seismology*. Editor G. Schubert (Amsterdam: Elsevier), 257–291. doi:10.1016/b978-0-44452748-6/00070-5
- INGV Seismological Data Centre (2006). *Rete Sismica Nazionale (RSN)*. Italy: Istituto Nazionale di Geofisica e Vulcanologia INGV.
- ISIDe Working Group (2007). *Italian Seismological Instrumental and Parametric Database (ISIDe)*. Italy: Istituto Nazionale di Geofisica e Vulcanologia INGV.
- Kilb, D. (2003). A strong Correlation between Induced Peak Dynamic Coulomb Stress Change from the 1992 M7.3 Landers, California, Earthquake and the Hypocenter of the 1999 M7.1 Hector Mine, California, Earthquake. *J. Geophys. Res.* 108 (B1), 2012. doi:10.1029/2001jb000678
- Kilb, D., Gomburg, J., and Bodin, P. (2002). Aftershock Triggering by Complete Coulomb Stress Changes. *J. Geophys. Res.* 107, 2060. doi:10.1029/2001jb000202
- King, G. C. P., and Devès, M. H. (2015). “Fault Interaction, Earthquake Stress Changes, and the Evolution of Seismicity,” in *Treatise on Geophysics Volume 4: Earthquake Seismology*. Editor G. Schubert (Amsterdam: Elsevier), 243–271. doi:10.1016/b978-0-444-53802-4.00077-4
- Lin, J., and Stein, R. (2004). Stress Triggering in Thrust and Subduction Earthquakes, and Stress Interaction between the Southern san Andreas and Nearby Thrust and Strike-Slip Faults. *J. Geophys. Res.* 109, B02303. doi:10.1029/2003jb002607
- Lomax, A., Michelini, A., and Curtis, A. (2009). Earthquake Location Earthquake Location, Direct, Global-Search Global-Search Methods. *Complexity Encyclopedia Complexity Syst. Sci.* 5, 2449–2473. doi:10.1007/978-0-387-30440-3
- Maestrelli, D., Benvenuti, M., Bonini, M., Carnicelli, S., Piccardi, L., and Sani, F. (2018). The Structural Hinge of a Chain-Foreland basin: Quaternary Activity of the Pede-Apennine Thrust Front (Northern Italy). *Tectonophysics*. 723, 117–135. doi:10.1016/j.tecto.2017.12.006
- Manga, M., Brumm, M., and Rudolph, M. L. (2009). Earthquake Triggering of Mud Volcanoes. *Mar. Pet. Geology*. 26, 1785–1798. doi:10.1016/j.marpetgeo.2009.01.019
- Manighetti, I., Campillo, M., Bouley, S., and Cotton, F. (2007). Earthquake Scaling, Fault Segmentation, and Structural Maturity. *Earth Planet. Sci. Lett.* 253 (3–4), 429–438. doi:10.1016/j.epsl.2006.11.004
- Marroni, M., Meneghini, F., and Pandolfi, L. (2017). A Revised Subduction Inception Model to Explain the Late Cretaceous, Double-Vergent Orogen in the Precollisional Western Tethys: Evidence from the Northern Apennines. *Tectonics*. 36, 2227–2249. doi:10.1002/2017TC004627
- Martini, I. P., and Sagri, M. (1993). Tectono-sedimentary Characteristics of Late Miocene-Quaternary Extensional Basins of the Northern Apennines, Italy. *Earth-Science Rev.* 34, 197–233. doi:10.1016/0012-8252(93)90034-5
- Michelini, A., Faenza, L., Lanzano, G., Lauciani, V., Jozinović, D., Puglia, R., et al. (2020). The New ShakeMap in Italy: Progress and Advances in the Last 10 Yr. *Seismological Res. Lett.* 91 (1), 317–333. doi:10.1785/0220190130
- Parsons, T. (2005). A Hypothesis for Delayed Dynamic Earthquake Triggering. *Geophys. Res. Lett.* 32, a–n. doi:10.1029/2004GL021811
- Piccinini, D., Piana Agostinetti, N., Saccorotti, G., Fiaschi, A., Matassoni, L., and Morelli, M. (2014). Orogen-parallel Variability in 3D Seismicity Distribution, Northern Apennines (Italy): Evidence for a Slab Tear Fault? *J. Geodynamics*. 82, 110–117. doi:10.1016/j.jog.2014.09.005
- Pizzi, A., Di Domenico, A., Gallovič, F., Luzi, L., and Puglia, R. (2017). Fault Segmentation as Constraint to the Occurrence of the Main Shocks of the 2016 Central Italy Seismic Sequence. *Tectonics*. 36, 2370–2387. doi:10.1002/2017TC004652
- Pondrelli, S., Morelli, A., Ekström, G., Mazza, S., Boschi, E., and Dziewonski, A. M. (2002). European-mediterranean Regional Centroid-Moment Tensors: 1997–2000. *Phys. Earth Planet. Interiors*. 130, 71–101. doi:10.1016/s0031-9201(01)00312-0
- Pondrelli, S., Salimbeni, S., Morelli, A., and Ekstrom, G. (2006). European-mediterranean Regional Centroid Moment Tensor Catalog: Solutions for Years 2003 and 2004. *Phys. Earth Planet. Int.* 159 (3–4), 286–303. doi:10.1016/j.pepi.2006.07.008
- Rösler, B., and Stein, S. (2022). Consistency of Non-double-couple Components of Seismic Moment Tensors with Earthquake Magnitude and Mechanism. *Seismol. Res. Lett.* XX, 1–14. doi:10.1785/0220210188
- Rovida, A., Locati, M., Camassi, R., Lolli, B., Gasperini, P., and Antonucci, A. (2021). *Catalogo Parametrico dei Terremoti Italiani (CPTI15), versione 3.0*. Italy: Istituto Nazionale di Geofisica e Vulcanologia INGV.
- Rovida, A., Locati, M., Camassi, R., Lolli, B., and Gasperini, P. (2020). The Italian Earthquake Catalogue CPTI15. *Bull. Earthquake Eng.* 18 (7), 2953–2984. doi:10.1007/s10518-020-00818-y
- Saccorotti, G., Piccinini, D., Mazzarini, F., and Zupo, M. (2013). Remotely Triggered Micro-earthquakes in the Larderello-Travale Geothermal Field (Italy) Following the 2012 May 20, Mw 5.9 Po-plain Earthquake. *Geophys. Res. Lett.* 40, 835–840. doi:10.1002/grl.50254
- Sani, F., Bonini, M., Montanari, D., Moratti, G., Corti, G., and Ventisette, C. D. (2016). The Structural Evolution of the Radicondoli–Volterra Basin (Southern Tuscany, Italy): Relationships With Magmatism and Geothermal Implications. *Geothermics*. 59, 38–55. doi:10.1016/j.geothermics.2015.10.008
- Sani, F., Bonini, M., Piccardi, L., Vannucci, G., Delle Donne, D., Benvenuti, M., et al. (2009). Late Pliocene-Quaternary Evolution of Outermost Hinterland Basins of the Northern Apennines (Italy), and Their Relevance to Active Tectonics. *Tectonophysics*. 476, 336–356. doi:10.1016/j.tecto.2008.12.012
- Scognamiglio, L., Tinti, E., and Michelini, A. (2009). Real-Time Determination of Seismic Moment Tensor for the Italian Region. *Bull. Seismological Soc. America*. 99 (4), 2223–2242. doi:10.1785/0120080104
- Scognamiglio, L., Tinti, E., and Quintiliani, M. (2006). *Time Domain Moment Tensor (TDMT) [Data Set]*. Italy: Istituto Nazionale di Geofisica e Vulcanologia INGV.
- Shang, J., Hencher, S. R., and West, L. J. (2016). Tensile Strength of Geological Discontinuities Including Incipient Bedding, Rock Joints and mineral Veins. *Rock Mech. Rock Eng.* 49 (11), 4213–4225. doi:10.1007/s00603-016-1041-x
- Stein, R. S. (1999). The Role of Stress Transfer in Earthquake Occurrence. *Nature*. 402, 605–609. doi:10.1038/45144
- Tarantola, A., and Valette, B. (1981). Inverse Problems = Quest for Information. *J. Geophys.* 50 (1), 159–170. Available at: <https://journal.geophysicsjournal.com/fofG/article/view/28>.
- Toda, S., Stein, R. S., Richards-Dinger, K., and Bozkurt, S. (2005). Forecasting the Evolution of Seismicity in Southern California: Animations Built on Earthquake Stress Transfer. *J. Geophys. Res.* 110, B05S16. doi:10.1029/2004jb003415
- van der Elst, N. J., and Brodsky, E. E. (2010). Connecting Near-Field and Far-Field Earthquake Triggering to Dynamic Strain. *J. Geophys. Res.* 115, B07311. doi:10.1029/2009JB006681
- Visini, F., Meletti, C., Rovida, A., D’Amico, V., Pace, B., and Pondrelli, S. (2022). Updated Area-Source Seismogenic Model for Seismic hazard of Italy. *Nat. Hazards Earth Syst. Sci. Discuss.* doi:10.5194/nhess-2022-60

- Waldhauser, F., and Ellsworth, W. L. (2000). A Double-Difference Earthquake Location Algorithm: Method and Application to the Northern Hayward Fault, California. *Bull. Seismological Soc. America*. 90, 1353–1368. doi:10.1785/0120000006
- Wells, D. L., and Coppersmith, K. J. (1994). New Empirical Relationships Among Magnitude, Rupture Length, Rupture Width, Rupture Area, and Surface Displacement. *Bull. Seismol. Soc. Am.* 84, 974–1002. doi:10.1785/BSSA0840040974

Conflict of Interest: The authors declare that the research was conducted in the absence of any commercial or financial relationships that could be construed as a potential conflict of interest.

Publisher's Note: All claims expressed in this article are solely those of the authors and do not necessarily represent those of their affiliated organizations, or those of the publisher, the editors and the reviewers. Any product that may be evaluated in this article, or claim that may be made by its manufacturer, is not guaranteed or endorsed by the publisher.

Copyright © 2022 Saccorotti, Bruni, Bonini, Corti, Keir and Sani. This is an open-access article distributed under the terms of the Creative Commons Attribution License (CC BY). The use, distribution or reproduction in other forums is permitted, provided the original author(s) and the copyright owner(s) are credited and that the original publication in this journal is cited, in accordance with accepted academic practice. No use, distribution or reproduction is permitted which does not comply with these terms.